Ellagic Acid

Contributor: Isabella Romeo

Polyphenol ellagic acid (EA) possesses antioxidant, anti-inflammatory, anti-carcinogenic, anti-diabetic and cardio protection activities, making it an interesting multi-targeting profile. EA also controls the central nervous system (CNS), since it was proven to reduce the immobility time of mice in both the forced swimming and the tail-suspension tests, with an efficiency comparable to that of classic antidepressants. The proposed mechanism revealed that EA mimics clonidine at the presynaptic release-regulating α2 autoreceptors in hippocampal noradrenergic nerve endings.

1. Introduction

Pomegranate (*Punica granatum* L.) is a very ancient edible fruit originating in the Middle East and North Africa, used from the dawn of history as a healing and health-promoting fruit in traditional medicine [1]. In the past decades, this rustic crop has obtained high popularity as a nutraceuticals source, becoming a high-value crop. Moreover, it has demonstrated increased importance due to its adaptability to different climatic conditions, its resilience and longevity, and its high drought and salinity resistance [2].

Today, pomegranate cultivation is widely spread in many tropical and subtropical regions, and about two million tons of fruits are produced annually worldwide [3]. Particularly, India, Iran, China, Turkey, the United States, Spain, South Africa, Peru, Chile, and Argentina represent the major producers and exporters of this fruit [4].

Pomegranate fruit is of great economic and nutritional interest, and it is in high demand due to its wide range of industrial uses, especially for direct consumption, for juice production, and oil extraction from its seeds [2]. The nutritional value of pomegranate is linked to its naturally high content of phenolic compounds with antioxidant properties [5]. Many studies, mainly in vitro, demonstrated the health benefits and the functional properties of this fruit in the prevention of several peripheral disorders such as cancer, cardiovascular diseases, chronic inflammatory diseases, and metabolic disorders (i.e., diabetes, obesity) [6]. Moreover, the beneficial effects of pomegranate phenolic compounds on central neuroinflammatory and neurodegenerative pathologies, including multiple sclerosis, Alzheimer's disease, Parkinson's diseases, epilepsy, and depression, have been highlighted too [7][8][9].

The main industrial product from pomegranate is its juice, obtained by aril squeezing, which represents the edible portion of the fruit, but recently there has been an increased focus on pomegranate by-products as a source of nutraceuticals. It has been determined that by-products, especially the peels, have higher levels of bioactive compounds and antioxidant activity than juice, opening new possibilities for pomegranate manufacturers to recover and exploit these by-products in a zero-waste economy perspective [10]. A major class of compounds in pomegranate fruit is the hydrolysable tannins, including ellagic acid, punicalagin, and gallic acid [11].

Ellagic acid (EA) is a chromene-dione derivative (3,7,8-tetrahydroxy-chromeno[5,4,3-cde]chromene-5,10-dione), which is derived from the spontaneously lactonization of hexahydroxydyphenic acid (HHDP) [12]. In its free form, or as constituent of ellagitannins (ETs), or conjugates with different monosaccharides (EA-glycosides), EA is considered the main phenolic compound responsible for the numerous health properties of pomegranate [12]. ETs are esters of gallic acid (GA) and hexahydroxydiphenic acid (HHDP) units, connected with mainly β-d-glucose as sugar residue. Punicalagin (2,3-(S)-hexahydroxydiphenoyl-4,6-(S,S)-gallagyl-d-glucose), a large molecule consisting of ellagic acid and gallagic acid linked via a glucose unit, is the most abundant ET in pomegranate and it is specific to the *Punica* genus [8]. Data from preclinical studies in the literature support the healthy properties of both EA and ETs. These include the ability to interfere with tumor cell proliferation, the cell cycle, invasion and angiogenesis by making it a multi-target candidate for various cancer treatments [13]. It also places a particular emphasis on the role of EA in central inflammatory and (auto)-immunological diseases, but also for depression, anxiety and aged-related neurological impairments [7][14][15][16] (**Figure 1**).
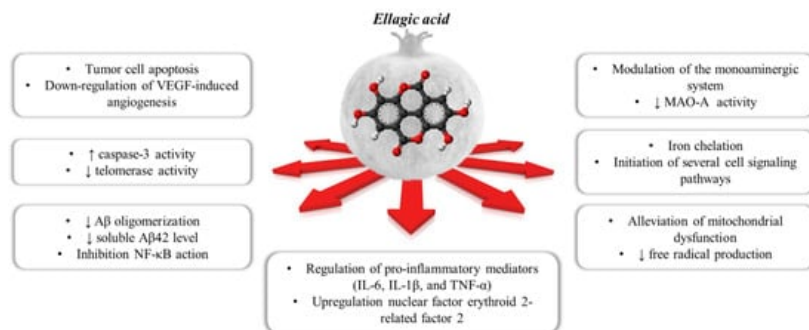
Figure 1. The polypharmacological effects regulated by ellagic acid contained within the pomegranate.

As far as the mood disorders are concerned, EA was proven to reduce the immobility time of mice in both the forced swimming and the tail-suspension tests, with an efficiency comparable to that of classic antidepressants [17]. Interestingly, the anti-depressant-like activity was almost nulled by the concomitant administration of selective antagonists of the noradrenergic receptors (namely the α_1, the α_2 and the β receptors) and by modulators of the serotonergic systems as well (including receptor antagonists and synthesis inhibitors) [17][18], suggesting the involvement of these cellular targets in the central effects elicited by EA and its derivatives.

Among the noradrenergic receptors, we focussed on the α_2 receptors (α_2-ARs) that, in the central nervous system (CNS), act as presynaptic inhibitory autoreceptors in noradrenergic nerve endings/varicosities [19][20]. The α_2-ARs are indirectly tuned by antidepressants acting as noradrenaline (NA) re-uptake inhibitors (NRI) [21]. By increasing NA bioavailability in the synaptic cleft, these drugs cause the continuous stimulation of the presynaptic α_2-Ars, leading to their down regulation. A comparable outcome also can be triggered by the continuous direct activation of the presynaptic α_2-ARs with agonists. In both cases, the final outcome is the silencing of the presynaptic mechanism of autocontrol of the release of the biogenic amine and, consequently, the reinforcement of the noradrenergic transmission [22][23][24]. Notably, the α_2-ARs also exist in astrocytes, where they control the phenotype of the glial cells favouring the non-inflammatory one [25]; whether and how these receptors desensitize was so far scarcely investigated.

The α_2-ARs are G protein coupled receptors (GPCRs) negatively associated to the adenylyl cyclase (AC) that reduce the gating of the voltage-operated calcium channels (VOCCs), concomitantly favouring the opening of the K^+-channels, to inhibit cellular functions. There are three characterized α_2-AR subtypes, the α_{2A}-AR, α_{2B}-AR and α_{2C}-AR [26], which are well conserved across mammals and are differently distributed in postganglionic sympathetic neurons and CNS noradrenergic neurons.

The α_{2A}-ARs and the α_{2C}-ARs are mainly expressed in noradrenergic neuronal projections from the Locus coeruleus to other central regions, with higher expression on the varicosities in dendritic and axonal processes, as well as in nerve terminals [20]. The α_{2A}-ARs and the α_{2C}-ARs are also present peripherally, on postganglionic sympathetic neurons, where again they act as inhibitory autoreceptors. Differently, the α_{2B}-ARs are preferentially expressed in the periphery, their presence in the CNS still representing a matter of debate [27].

2. Computational Studies

In silico studies were carried out to explore the binding modes of EA into α_{2A}-ARs and α_{2C}-AR catalytic pockets. In addition to this, these specific docking studies were carried out to investigate the possible differences and similarities of the interactions established between a known agonist (clonidine) or antagonist (yohimbine) with the receptors. For the current analysis, the crystal structures of the human α_{2A}-AR in complex with the indole derivative, a partial agonist (PDB code: 6KUY) [28], α_{2A}-AR in complex with the naphthyridine derivative, an antagonist (PDB code: 6KUX) [29], and, α_{2C}-AR in complex with the naphthyridine derivative, an antagonist (PDB code: 6KUW [30], were used.

2.1. Molecular Docking Studies

For each structure, the docking protocol was validated by docking the co-crystallized ligand into the binding site (**Figure 2**a,b). Root mean square deviation (RMSD) values between the native pose of α_{2A}-AR$_{6KUY}$, α_{2A}-AR$_{6KUX}$ and α_{2C}-AR$_{6KUW}$ ligands and the related best re-docked conformations were found to be 0.19 Å (**Figure 2**c), 0.89 Å (**Figure 2**d), and 0.39 Å (**Figure 2**e), respectively, thus revealing the reliability of docking protocol (**Figure 2**a–c).
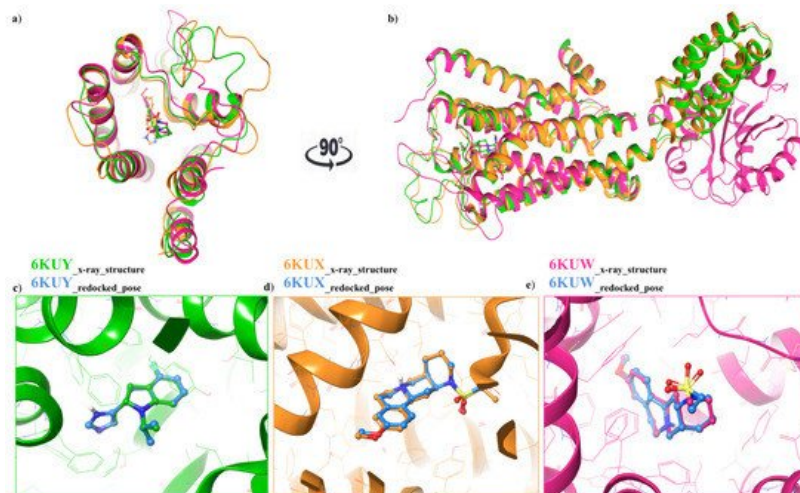
Figure 2. (**a**) Top view: Ribbon representation of overlaid binding orientation of co-crystallized ligands into the binding site of α_{2A}-AR$_{6KUY}$ (orange), α_{2A}-AR$_{6KUX}$ (green) and α_{2C}-AR$_{6KUW}$ (magenta) structures; (**b**) Front view of the superposed $\alpha_{2A\text{-}C}$-ARSs. Three-dimensional superimposition between the re-docked pose (blue carbon ball and sticks) and the conformation of the native ligand; (**c**) Indole derivative into the binding site of 6KUY; (**d**) Naphthyridine derivative into both 6KUX (green) and (**e**) 6KUW (magenta) X-ray structures.

The three ligands were docked to the minimized structures of the α_2-ARs subtypes A and C, respectively (**Table 1**). Regarding yohimbine in complex to α_{2A}-AR$_{6KUX}$, it was observed that it was able to better recognize the orthosteric pocket of the receptor, compared to EA and clonidine. In detail, the positively charged amine group in the pyrido[1,2-b]isoquinoline displays a hydrogen bond with D113 (1.81 Å) and a π-cation interaction with F412. The hydroxyl and the carboxylic group create a hydrogen bond with Y98 side chain and I190 backbone, respectively. Furthermore, the indole moiety enhances the binding by two π-π interactions with F390 and F391 (**Figure 3**g–i).
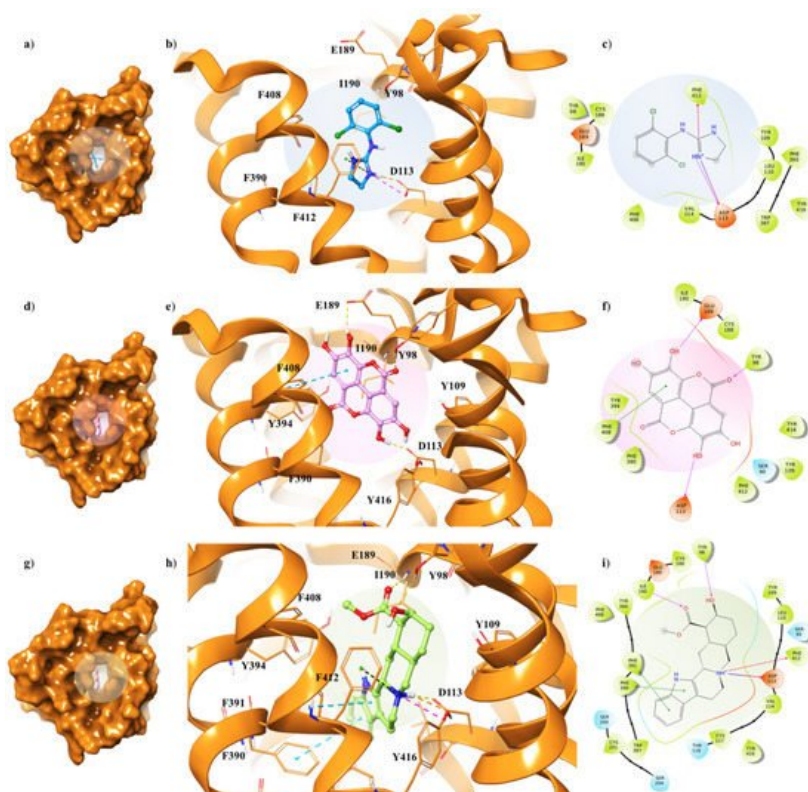
Figure 3. Key contacting elements inside (**a**–**c**) the α_{2A}-AR$_{6KUX}$/clonidine, (**d**–**f**) the α_{2A}-AR$_{6KUX}$/EA, and (**g**–**i**) the α_{2A}-AR$_{6KUX}$/yohimbine best docked pose. Panels (**b**,**e**,**h**) show all side chains involved in H-bonds (violet), π-π interactions (cyan) and π-cation interactions (red) in stick representation. Panels (**a**,**d**,**g**) show the surface area of α_{2A}-AR$_{6KUX}$ complexed to clonidine, EA and yohimbine, respectively. The surface area of the receptor is shown in solid orange solid. 2D representation of the key interactions of (**c**) clonidine, (**f**) EA and (**i**) yohimbine into the α_{2A}-AR$_{6KUY}$ structure.

Table 1. Glide score, calculated in kcal/mol, of the best yohimbine, EA and clonidine docked pose towards α_{2A}-AR$_{6KUX}$, α_{2A}-AR$_{6KUY}$ and α_{2C}-AR$_{6KUW}$ structures.

| | α$_{2A}$-AR$_{6KUX}$ | α$_{2A}$-AR$_{6KUY}$ | α$_{2C}$-AR$_{6KUW}$ |
	Glide SP Score *	Glide SP Score *	Glide SP Score *
Yohimbine	−7.86	−7.62	−9.12
EA	−6.56	−7.43	−5.61
Clonidine	−4.85	−6.02	−4.39

* Glide SP score is calculated in kcal/mol.

The peculiar structure of the EA is buried in a hydrophobic core formed by Y98, Y109, I190, F390, Y394, F408, F412 and Y416 residues (**Figure 3**f). The receptor–ligand interaction is then stabilized by H-bond interactions between the hydroxyl groups of the two gallic acid motifs and the side chains of D113 and E189, which lie on the extracellular loop 2 (XL2), directly linked to the TM5 [31]. Furthermore, a π-π interaction occurs in proximity with the receptor exterior, between F408 and one of the aryl rings; meanwhile, the oxygen of the carbonyl group of the EA forms the hydrogen bond with the hydroxyl group of Y98 (**Figure 3**d,e).

Clonidine docking pose shows a very similar orientation to that of the EA into the α$_{2A}$-AR$_{6KUX}$ binding cavity, thus pointing the positive charge of the imidazole ring towards D113 and F412, through a H-bond and a π-cation interaction, respectively, acting as an anchor within the binding site (**Figure 3**a–c).

Although α$_{2A}$-AR$_{6KUX}$ and α$_{2A}$-AR$_{6KUY}$ are characterized by a different rearrangement of the side chains of the hydrophobic residues into the binding pocket, the indole moiety of the yohimbine into α$_{2A}$-AR$_{6KUY}$ can create a π-π interaction with F412 and W438 (**Figure 4**g–i). Instead, EA interacts with F391 and Y394 by means of one gallic acid motif (**Figure 4**d–f). When clonidine is docked to α$_{2A}$-AR$_{6KUY}$, the 2-aminoimidazoline group forms two hydrogen bonds with D113, and a π-cation interaction with F390, while the dichlorophenyl ring stretches towards the extracellular solvent to bind the Y394 residue (**Figure 4**a–c).
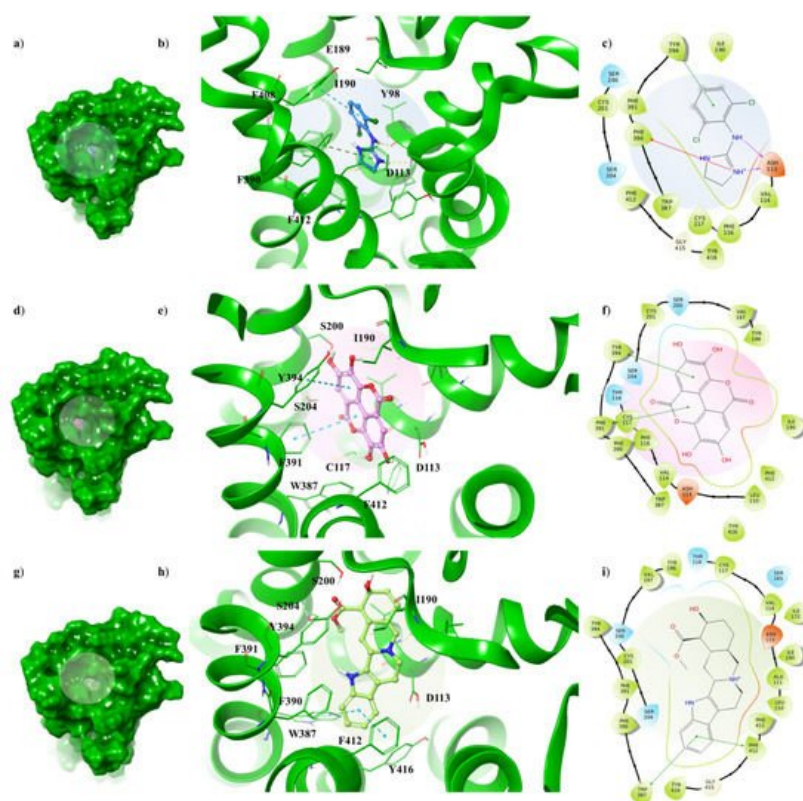
Figure 4. Key contacting elements inside (**a**–**c**) the α$_{2A}$-AR$_{6KUY}$/clonidine, (**d**–**f**) the α$_{2A}$-AR$_{6KUY}$/EA, and (**g**–**i**) the α$_{2A}$-AR$_{6KUY}$/yohimbine best docked pose. Panels (**b**,**e**,**h**) show all side chains involved in H-bonds (violet), π-π interactions (cyan) and π-cation interactions (red) in stick representation. Panels (**a**,**d**,**g**) show the surface area of α$_{2A}$-AR$_{6KUY}$ complexed to clonidine, EA and yohimbine, respectively. The surface area of the receptor is shown in solid green. 2D representation of the key interactions of (**c**) clonidine, (**f**) EA and (**i**) yohimbine into the α$_{2A}$-AR$_{6KUY}$ structure.

Concerning the α$_{2C}$-AR$_{6KUW}$ subtype, docking analysis highlights that yohimbine forms a conserved salt bridge with the carboxylate of D131 and, also, a π-cation interaction with F423 and F391 (**Figure 5**a–c).
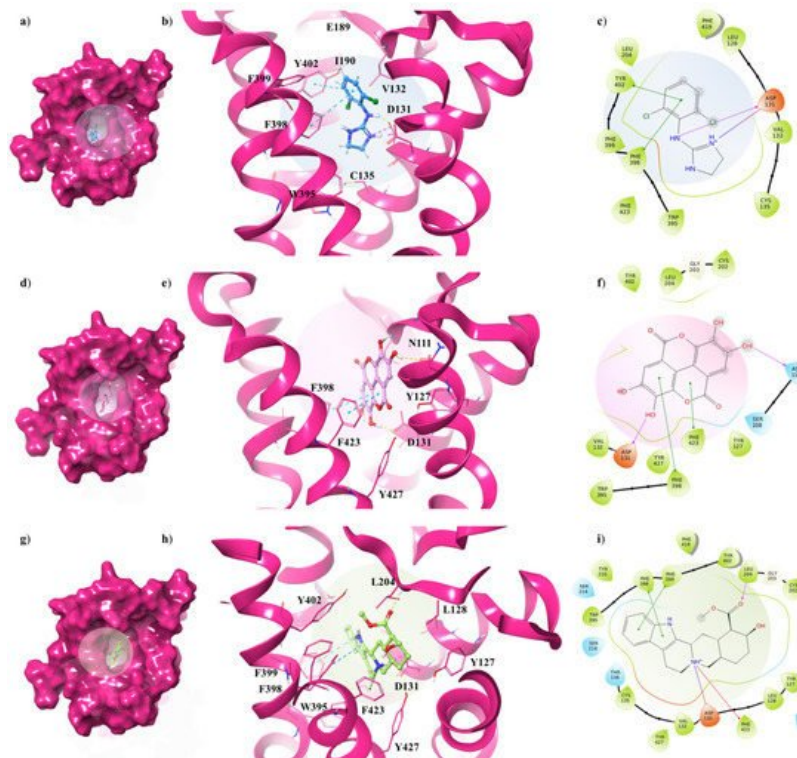
Figure 5. Key contacting elements inside (**a**–**c**) the α_{2A}-AR$_{6KUW}$/clonidine, (**d**–**f**) the α_{2A}-AR$_{6KUW}$/EA, and (**g**–**i**) the α_{2A}-AR$_{6KUW}$/yohimbine best docked pose. Panels (**b**,**e**,**h**) show all side chains involved in H-bonds (violet), π-π interactions (cyan) and π-cation interactions (red) in stick representation. Panels (**a**,**d**,**g**) show the surface area of α_{2A}-AR$_{6KUW}$ complexed to clonidine, EA and yohimbine, respectively. The surface area of the receptor is shown in solid magenta. 2D representation of the key interactions of (**c**) clonidine, (**f**) EA and (**i**) yohimbine into α_{2A}-AR$_{6KUY}$ structure.

The antagonist is surrounded by nine aromatic residues (Y127, Y210, W395, F398, F399, Y402, F419, F423, Y427) on TM6 and TM7, and three other residues (L128, V132, L204) forming the hydrophobic environment of the binding cavity. The indole moiety interacts with F398 and F399 by means of two π-π interactions, while the carboxyl group engages a H-bond with L204, one of the pivotal residues in establishing subtype selectivity [32].

EA is well accommodated into the α_{2C}-AR pocket and interacts with the same residues with which yohimbine interacts, except that one hydroxyl group of EA is in contact with N111 (**Figure 5**d–f). Finally, analysing the interactions between clonidine and α_{2C}-AR$_{6KUW}$, it is noted that the 2-aminoimidazoline group creates two hydrogen bonds with D131, and then the dichlorophenyl ring is stabilized by two π-π interactions with F398 and Y402 (**Figure 5**g–i).

2.2. MDs of EA Complexed with α_2-ARs

For each complex, the best docked pose of EA, yohimbine and clonidine into α_2-ARs binding pockets were chosen as the starting point for 50 ns of molecular dynamics simulations (MDs). MDs results were investigated in terms of stability of the complexes and conformational flexibility of α_2-ARs in presence of the EA, with respect to the partial agonist and the antagonist, such as the clonidine and the yohimbine, respectively, by monitoring the single contributions of hydrophobic, water bridges and hydrogen bonding interactions.

In order to hypothesize the partial agonist or antagonist activity of EA, based on the importance of the interaction with aspartic acid on TM3 and the serine residues contained in TM5, as reported in previous studies [33], we monitored the distance between the centroid atom of EA, clonidine and yohimbine structures and the Cα of these critical residues, in α_{2A} (D113, S200, S204) and α_{2C} (D131, S214, S218) adrenoreceptors. Particularly, for the α_{2A}-AR structure, a lower distance between EA and S200 was found with respect to that of clonidine and yohimbine (**Figure 6**a), with the average values equal to 7.3 Å, 10.0 Å and 10.8 Å, respectively. As already understood, S200 and S204 play a crucial role in the activation of aminergic GPCRs such as the α_2-AR. The lack of flexibility of EA and its peculiar structure with hydrophobic core and hydrophilic ends allow it to reside in the TM5 area, which may be the cause of its partial agonism compared to the antagonist profile of yohimbine, which seems to move away from the TM5 in the last 10 ns of dynamics. Meanwhile, for the α_{2C}-AR structure, all three investigated compounds remain stable in the orthosteric binding pocket (**Figure 6**b). No significant differences can be observed, except for EA which seems to be prone towards S214 at the end of the MDs.
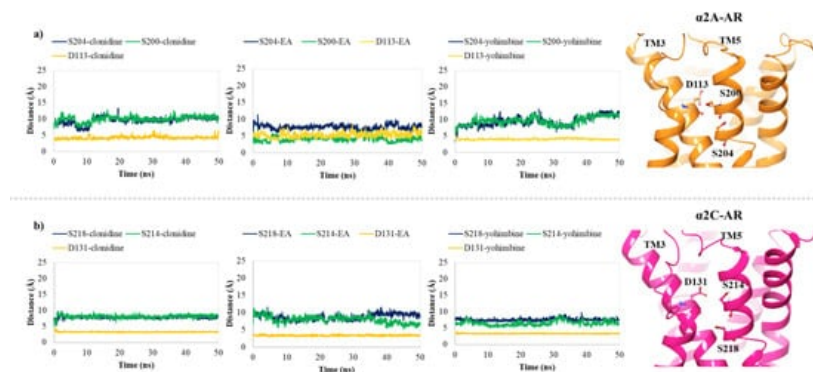
Figure 6. Plots of the distances between the centroid atom of EA, clonidine and yohimbine and (**a**) D113 (orange), S200 (green) and S204 (blue) into the α_{2A}-AR structure; (**b**) D131 (orange), S214 (green), and S218 (blue) into the α_{2C}-AR structure, throughout 50 ns of MDs. Right-hand images show zoomed-in context of the pivotal residues, depicted in orange and magenta carbon ball and sticks, involved in the α_{2A}-AR and α_{2C}-AR binding pockets, respectively.

Taking into account the dynamic behaviour of EA into the α_{2A}-AR$_{6KUX}$ structure with respect to the agonist and the antagonist, it is noticed that EA shifts towards R405 to form a π-cation interaction for 31% of MDs, losing the initial binding to D113. Its hydroxyl groups bind S90 and Y109 for 24% and 25% of MDs, respectively. Trajectories of clonidine and yohimbine present some similarities, such as their ability to interact with D113, Y394 and F412 residues, with an additional water bridge and H-bond with the E189 (36%) and I190 (95%) for the yohimbine in the complex with α_{2A}-AR$_{6KUX}$. Meanwhile, S200, which belongs to the TM5, stabilizes the clonidine into the α_{2A}-AR$_{6KUX}$ pocket by means of a water-bridge for 46% of MDs, underlining the key binding elements in common to the endogenous ligands and, consequently, its role as a partial agonist.

Curiously, even if EA is not able to maintain the interaction with D113, it is well stabilized during the whole trajectory in the complex with the α_{2A}-AR$_{6KUY}$ structure. Its conformational restraint provided by the hydrophobic core and the presence of the four hydroxyl groups results in a stronger binding affinity to drive EA within the α_{2A}-AR$_{6KUY}$ pocket for a good anchoring system than that of both the partial agonist and antagonist structures. Indeed, aromatic residues such as F116 and F390 form π-π interactions with the gallic acid motifs of EA for 38% and 98% of MDs. Moreover, S204, F408, F410 and F412 residues show a water-bridge interaction for around 30–60% of the trajectory. Regarding clonidine-α_{2A}-AR$_{6KUY}$ complex MDs, the 2-aminoimidazoline group binds D113 (30%) and F414 (33%) through an H-bond and a π-cation interaction, respectively. Additionally, the dichlorophenyl ring is oriented between Y394 and F391, engaging π-π interactions for a half run of MDs. Instead, analysing MDs of yohimbine-α_{2A}-AR$_{6KUY}$, its major flexibility allows maintenance of the interaction between the positively charged amine group in the pyrido[1,2-b]isoquinoline and D113 (38%) and L110 (53%) residues. This moiety also forms the successful anchoring π-π interaction with the phenylalanine at position 390 and 391 for 34% and 45% of MDs, respectively.

Conversely, all the three investigated compounds interact with similar but non identical subsets of residues in the α_{2C}-AR structure. In particular, during the whole simulation, it can be observed that the 2-aminoimidazoline group of clonidine, the pyrido[1,2-b]isoquinoline of the yohimbine, and the two hydroxyl groups of one gallic acid motif of EA participate in the pivotal interaction with the side chain oxygens of D131 (**Figure 4**b), which is involved in adrenergic signalling for 96%, 99% and 99% of MDs, respectively. Y402 also provides a significant π-cation with clonidine (48%) and π-π interactions with both EA (40%) and yohimbine (42%). One gallic motif in EA displays two π-cation interactions with K420 for 55% and 31% of MDs. Carefully looking at yohimbine accommodation into the α_{2C}-AR pocket during MDs, it appears that the indole moiety and the carboxyl group participate in major interactions with F398 (57%), and L204 (65%), respectively. Moreover, the hydroxyl group of yohimbine displays one water bridge with E112 (54%).

Finally, the binding free energies calculated by carrying out the MM/GBSA method, known to be one of the rigorous and efficient methods to predict relative binding affinities, has been useful for evaluating the strength of EA's affinity over the α_2-ARs binding pocket [34][35][36][37][38][39][40][41][42][29][43]. In this way, 1000 snapshots from 50 ns of MDs are extracted for the binding free energy calculations of both the α_2-ARs-EA complex and the known partial agonist and antagonist in complex to α_2-ARs [44][45]. The results of the calculated free energy trends for EA, in comparison with clonidine and yohimbine, are reported in **Figure 7**a–c.
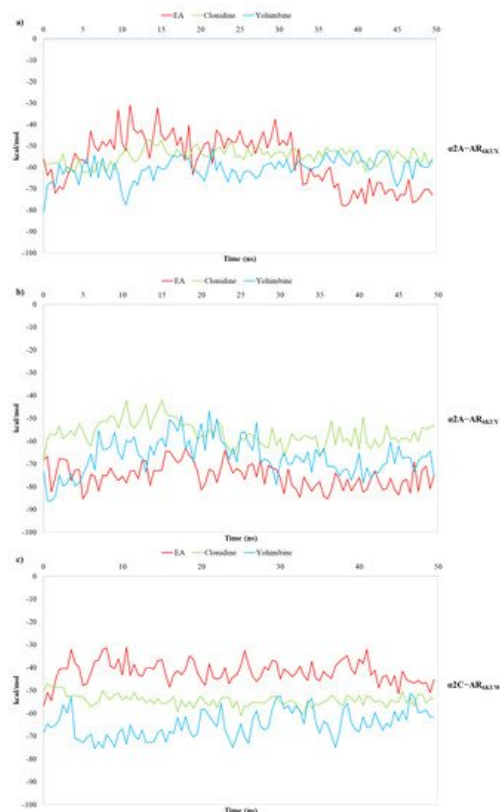
Figure 7. Plots of MM/GBSA trend for EA, clonidine and yohimbine in complex to (**a**) α_{2A}-AR$_{6KUX}$, (**b**) α_{2A}-AR$_{6KUY}$, and (**c**) α_{2C}-AR$_{6KUW}$, during 50 ns of MDs.

MM/GBSA analysis reveals that the average calculated binding free energies (ΔG_{bind}) of EA, clonidine and yohimbine complexed with α_{2A}-AR$_{6KUX}$ (**Figure 6**a) are −57.02, −54.86 and −60.69 kcal/mol, respectively, during the whole trajectories. Looking at the MM/GBSA trend, it can be seen that EA may behave like a partial agonist, strengthening its non-bonded interactions throughout MDs. Instead, the average values of −75.22, −56.41, −66.89 kcal/mol are calculated for EA, clonidine and yohimbine into α_{2A}-AR$_{6KUY}$, respectively, thus resulting in a more stabilizing effect of EA over the pocket of α_{2A}-ARs (**Figure 6**b). In the α_{2C}-AR$_{6KUW}$, the MM/GBSA trend shows that yohimbine is associated to the higher binding free energies than that of both clonidine and EA, with average values equal to −64.88, −54.29 and −42.00 kcal/mol, respectively (**Figure 7**c).

3. Pharmacological In Vitro Functional Studies

3.1. α_{2A} and α_{2C} Receptor Proteins in Hippocampal Lysates

The ascending noradrenergic projections from the Locus coeruleus to the hippocampus possess in their preterminal varicosities and terminals presynaptic inhibitory release-regulating α_2-ARs, as confirmed by the Western blot analysis of the mouse hippocampal lysates, which demonstrated the presence of the α_{2A}-AR (**Figure 8**A) and the α_{2C}-AR (**Figure 8**B) proteins, having a mass consistent with the monomeric structure (45 kDa and 50 kDa for the α_{2A} and α_{2C} receptor proteins, respectively), but also of polymeric associations, particularly evident in the case of α_{2A}-AR. The analysis unveiled a direct correlation between the intensity of the immune-positivities and the protein content loaded in each lane. We did not investigate the presence of the α_{2B}-AR protein because of its preferential peripheral expression [46].
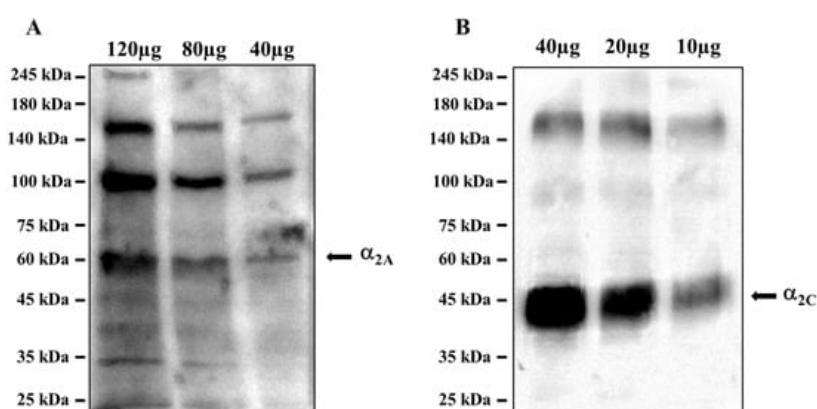
Figure 8. Mouse hippocampal lysates are endowed with (**A**) the α_{2A}-AR and (**B**) the α_{2C}-AR proteins. The images are representative of three analyses run on different preparations. Protein weights are expressed in kDa.

These results confirmed the presence of α_{2A}-AR and α_{2C}-AR proteins in the hippocampus of adult mice, opening the possibility to focus on this brain region for in vitro functional studies to verify the intrinsic activity of EA on naïve α_2-ARs.

3.2. Ellagic Acid Mimics Clonidine at the Presynaptic Release-Regulating α_2 Autoreceptors in Hippocampal Noradrenergic Nerve Endings: Antagonism by Yohimbine

To verify, by a functional point of view, if naive α_2ARs could represent a specific cellular target of EA, we isolated synaptosomes from the hippocampus of adult male mice, and quantified in release experiments the impact of EA on the NA exocytosis. Experiments were carried out by using the technique of the "up-down superfusion of a thin layer of synaptosomes", which is widely recognized as an approach of choice to prove, by a functional point of view, the existence of receptors in nerve endings, and to pharmacologically characterize the affinity and the intrinsic activity of ligand(s) acting at selected naïve receptor subtypes (see for experimental and technical details in the Method section, **Figure 9**).
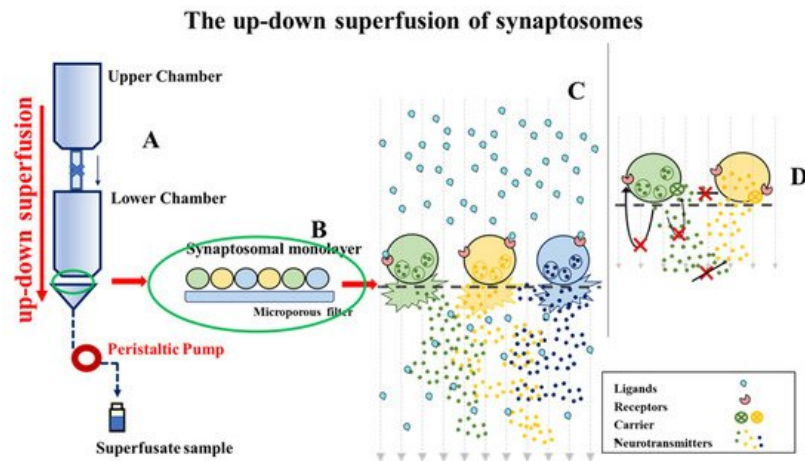
Figure 9. The superfusion apparatus (see text) [39][40].

Consistent with the inhibitory nature of the presynaptic α_2-ARs, the exocytotic-like release of preloaded [^{3}H]NA elicited by 12 mM KCl-enriched solution was significantly reduced (-48.80%, $n = 4$, $p < 0.05$, result expressed as % of inhibition) when the α_2-ARs agonist clonidine (0.1 µM) was added concomitantly to the depolarizing stimulus. An almost comparable reduction of [^{3}H]NA exocytosis was observed when synaptosomes were exposed to the KCl-enriched solution containing 10 nM EA (-36.80, $n = 5$, $p < 0.05$); a lower concentration (1 nM) of the natural compound slightly, although not significantly (-13.74, $n = 3$, n.s.), affected the tritium overflow (**Figure 10**a).
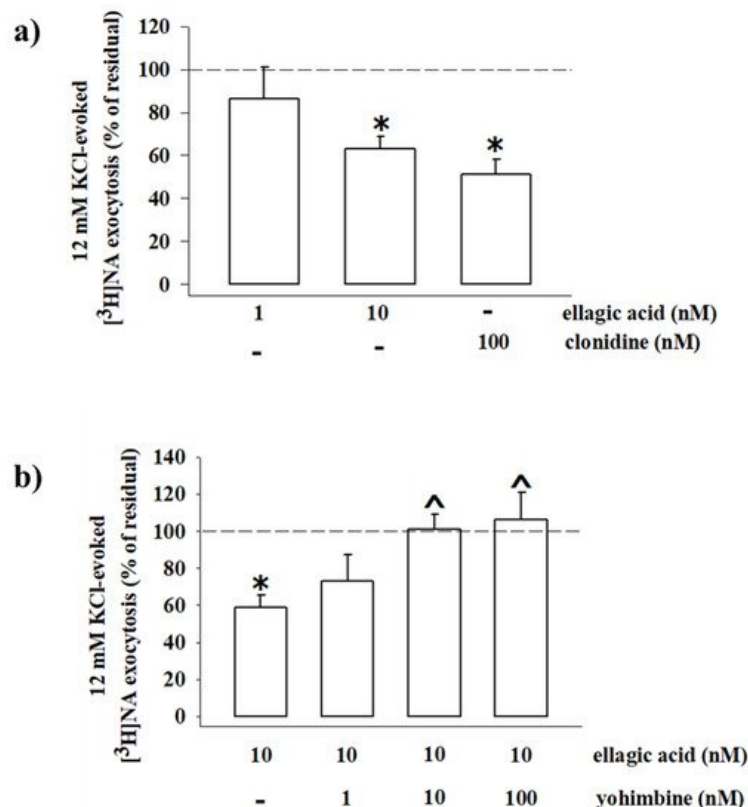
Figure 10. Ellagic acid mimics clonidine in inhibiting the [3][H]noradrenaline ([3][H]NA) exocytosis from mouse hippocampal synaptosomes, and its effect is reversed by yohimbine. (**a**) Effects of ellagic acid (1 and 10 nM) and clonidine (100 nM) on the 12 mM KCl-evoked [3][H]NA release from mouse hippocampal synaptosomes. (**b**) Effect of ellagic acid (10 nM), alone or concomitantly added with yohimbine (1–100 nM), on the 12 mM KCl-evoked [3][H]NA release from mouse hippocampal synaptosomes. Results are expressed as percentage of residual of the 12 mM KCl-evoked tritium release. Data represent the means ± SEM of four to five experiments run in triplicate. * $p < 0.05$ versus 12 mM KCl-induced tritium overflow; ^ $p < 0.05$ versus 12 mM KCl/10 nM ellagic acid-induced tritium overflow.

References

1. Barbieri, M.; Heard, C.M. Isolation of punicalagin from Punica granatum rind extract using mass-directed semi-preparative ESI-AP single quadrupole LC-MS. J. Pharm. Biomed. Anal. 2019, 166, 90–94.

2. Turrini, F.; Malaspina, P.; Giordani, P.; Catena, S.; Zunin, P.; Boggia, R. Traditional decoction and PUAE aqueous extracts of pomegranate peels as potential anti-tyrosinase ingredients. Appl. Sci. 2020, 10, 2795.

3. Global Pomegranate Market Industry Trends, Sales, Supply, Demand, Analysis & Forecast. 2017. Available online: https://www.researchmoz.us/global-pomegranate-market-2017-industry-trends-sales-supply-demand-analysis-and-forecast-to-2022-report.html (accessed on 17 November 2020).

4. Shahkoomahally, S.; Khadivi, A.; Brecht, J.K.; Sarkhosh, A. Chemical and physical attributes of fruit juice and peel of pomegranate genotypes grown in Florida USA. Food Chem. 2020, 342, 128302.

5. Ifeanyichukwu, U.L.; Fayemi, O.E.; Ateba, C.N. Green Synthesis of Zinc Oxide Nanoparticles from Pomegranate (Punica granatum) Extracts and Characterization of Their Antibacterial Activity. Molecules 2020, 25, 4521.

6. Zuccari, G.; Baldassari, S.; Ailuno, G.; Turrini, F.; Alfei, S.; Caviglioli, G. Formulation strategies to improve oral bioavailability of ellagic acid. Appl. Sci. 2020, 10, 3353.

7. Ahmed, T.N.; Setzer, W.; Fazel Nabavi, S.; Erdogan Orhan, I.; Braidy, N.; Sobarzo-Sanchez, E.; Mohammad Nabavi, S. Insights into Effects of Ellagic Acid on the Nervous System: A Mini Review. Curr. Pharm. Des. 2016, 22, 1350–1360.

8. Alfei, S.; Turrini, F.; Catena, S.; Zunin, P.; Grilli, M.; Pittaluga, A.; Boggia, R. Ellagic Acid a multi-target bioactive compound for drug discovery in CNS? A narrative review. Eur. J. Med. Chem. 2019, 183, 111724.

9. Boggia, R.; Turrini, F.; Roggeri, A.; Olivero, G.; Cisani, F.; Bonfiglio, T.; Summa, M.; Grilli, M.; Caviglioli, G.; Alfei, S.; et al. Neuroinflammation in Aged Brain: Impact of the Oral Administration of Ellagic Acid Microdispersion. Int. J. Mol. Sci. 2020, 21, 3631.

10. Magangana, T.P.; Makunga, N.P.; Fawole, O.A.; Opara, U.L. Processing Factors Affecting the Phytochemical and Nutritional Properties of Pomegranate (Punica granatum L.) Peel Waste: A Review. Molecules 2020, 25, 4690.

11. Turrini, F.; Boggia, R.; Donno, D.; Parodi, B.; Beccaro, G.L.; Baldassari, S.; Signorello, M.G.; Catena, S.; Alfei, S.; Zunin, P. From pomegranate marcs to a potential bioactive ingredient: A recycling proposal for pomegranate-squeezed marcs. Europ. Food Res. Technol. 2020, 246, 273–285.

12. Turrini, F.; Zunin, P.; Catena, S.; Villa, C.; Alfei, S.; Boggia, R. Traditional or hydro-diffusion and gravity microwave coupled with ultrasound as green technologies for the valorization of pomegranate external peels. Food Bioprod. Process. 2019, 117, 30–37.

13. Kim, S.A.; Go, A.; Jo, S.H.; Park, S.J.; Jeon, Y.U.; Kim, J.E.; Lee, H.K.; Park, C.H.; Lee, C.O.; Park, S.G.; et al. A novel cereblon modulator for targeted protein degradation. Eur. J. Med. Chem. 2019, 15, 65–74.

14. Ríos, J.L.; Giner, R.M.; Marín, M.; Recio, M.C. A Pharmacological Update of Ellagic Acid. Planta Med. 2018, 84, 1068–1093.

15. Saeed, M.; Naveed, M.; BiBi, J.; Kamboh, A.A.; Arain, M.A.; Shah, Q.A.; Alagawany, M.; El-Hack, M.E.A.; Abdel-Latif, M.A.; Yatoo, M.I.; et al. The Promising Pharmacological Effects and Therapeutic/Medicinal Applications of Punica granatum L. (Pomegranate) as a Functional Food in Humans and Animals. Recent Pat. Inflamm. Allergy Drug Discov. 2018, 12, 24–38.

16. De Oliveira, M.R. The Effects of Ellagic Acid upon Brain Cells: A Mechanistic View and Future Directions. Neurochem. Res. 2016, 41, 1219–1228.

17. Girish, C.; Raj, V.; Arya, J.; Balakrishnan, S. Evidence for the involvement of the monoaminergic system, but not the opioid system in the antidepressant-like activity of ellagic acid in mice. Eur. J. Pharmacol. 2012, 682, 118–125.

18. Bhargava, U.C.; Westfall, B.A. The mechanism of blood pressure depression by ellagic acid. Proc. Soc. Exp. Biol. Med. 1969, 132, 754–756.

19. Trendelenburg, A.U.; Philipp, M.; Meyer, A.; Klebroff, W.; Hein, L.; Starke, K. All three alpha2-adrenoceptor types serve as autoreceptors in postganglionic sympathetic neurons. Naunyn Schmiedebergs Arch. Pharmacol. 2003, 368, 504–512.

20. Langer, S.Z. Presynaptic autoreceptors regulating transmitter release. Neurochem. Int. 2008, 52, 26–30.

21. Schramm, N.L.; McDonald, M.P.; Limbird, L.E. The α2A-adrenergic receptor plays a protective role in mouse behavioral models of depression and anxiety. J. Neurosci. 2001, 21, 4875–4882.

22. Pittaluga, A.; Raiteri, L.; Longordo, F.; Luccini, E.; Barbiero, V.S.; Racagni, G.; Popoli, M.; Raiteri, M. Antidepressant treatments and function of glutamate ionotropic receptors mediating amine release in hippocampus. Neuropharmacology 2007, 53, 27–36.

23. Vizi, E.S.; Kiss, J.P.; Lendvai, B. Nonsynaptic Communication in the Central Nervous System. Neurochem. Int. 2004, 45, 443–451.

24. Jiang, J.L.; El Mansari, P.; Blier, M. Triple reuptake inhibition of serotonin, norepinephrine, and dopamine increases the tonic activation of α2-adrenoceptors in the rat hippocampus and dopamine levels in the nucleus accumbens. Prog. Neuropsychopharmacol. Biol. Psychiatry 2020, 103, 109987.

25. Giorgi, F.S.; Biagioni, F.; Galgani, A.; Pavese, N.; Lazzeri, G.; Fornai, F. Locus Coeruleus Modulates Neuroinflammation in Parkinsonism and Dementia. Int. J. Mol. Sci. 2020, 21, 8630.

26. Harrison, J.K.; Pearson, W.R.; Lynch, K.R. Molecular characterization of alpha 1- and alpha 2-adrenoceptors. Trends Pharmacol. Sci. 1991, 12, 62–67.

27. Trendelenburg, A.U.; Klebroff, W.; Hein, L.; Starke, K. A study of presynaptic α2-autoreceptors in α2A/D-, α2B- and α2C-adrenoceptor-deficient mice. Naunyn-Schmiedeberg's Arch. Pharmacol. 2001, 364, 117–130.

28. Qu, L.; Zhou, Q.T.; Xu, Y.; Guo, Y.; Chen, X.Y.; Yao, D.; Han, G.W.; Liu, Z.-J.; Stevens, R.C.; Zhong, G.S.; et al. Structural basis of the diversity of adrenergic receptors. Cell Rep. 2019, 29, 2929–2935.

29. Qu, L.; Zhou, Q.T.; Wu, D.; Zhao, S.W. Crystal structures of the alpha2A adrenergic receptor in complex with an antagonist RSC. Released Protein Data Bank 2019.

30. Chen, X.Y.; Wu, D.; Wu, L.J.; Han, G.W.; Guo, Y.; Zhong, G.S. Crystal structure of human alpha2C adrenergic G protein-coupled receptor. Released Protein Data Bank 2019.

31. Schneider, J.; Korshunova, K.; Musiani, F.; Alfonso-Prieto, M.; Giorgetti, A.; Carloni, P. Predicting ligand binding poses for low-resolution membrane protein models: Perspectives from multiscale simulations. Biochem. Biophys. Res. Comm. 2018, 498, 366–374.

32. Chen, X.; Xu, Y.; Qu, L.; Wu, L.; Han, G.W.; Guo, Y.; Wu, Y.; Zhou, Q.; Sun, Q.; Chu, C.; et al. Molecular Mechanism for Ligand Recognition and Subtype Selectivity of α2C Adrenergic Receptor. Cell Rep. 2019, 29, 2936–2943.e4.

33. McMullan, M.; Kelly, B.; Mihigo, H.B.; Keogh, A.P.; Rodriguez, F.; Brocos-Mosquera, I.; García-Bea, A.; Miranda-Azpiazu, P.; Callado, L.F.; Rozas, I. Di-aryl guanidinium derivatives: Towards improved α2-Adrenergic affinity and antagonist activity. Europ. J. Med. Chem. 2021, 209, 112947.

34. Hou, T.J.; Wang, J.M.; Li, Y.Y.; Wang, W. Assessing the performance of the MM/PBSA and MM/GBSA methods. 1. The accuracy of binding free energy calculations based on molecular dynamics simulations. J. Chem. Inf. Model. 2011, 51, 69–82.

35. Kopitz, H.; Cashman, D.A.; Pfeiffer-Marek, S.; Gohlke, H. Influence of the solvent representation on vibrational entropy calculations: Generalized Born versus distance-dependent dielectric model. J. Comput. Chem. 2012, 12, 1004–1013.

36. Genheden, S.; Ryde, U. The MM/PBSA and MM/GBSA methods to estimate ligand-binding affinities. Expert Opin. Drug Discov. 2015, 10, 449–461.

37. Olivero, G.; Cisani, F.; Marimpietri, D.; Di Paolo, D.; Gagliani, M.C.; Podestà, M.; Cortese, K.; Pittaluga, A. The Depolarization-Evoked, Ca2+-Dependent Release of Exosomes from Mouse Cortical Nerve Endings: New Insights into Synaptic Transmission. Front. Pharmacol. 2021, 22, 670158.

38. Olivero, G.; Bonfiglio, T.; Vergassola, M.; Usai, C.; Riozzi, B.; Battaglia, G.; Nicoletti, F.; Pittaluga, A. Immuno-pharmacological characterization of group II metabotropic glutamate receptors controlling glutamate exocytosis in mouse cortex and spinal cord. Br. J. Pharmacol. 2017, 174, 4785–4796.

39. Raiteri, M.; Angelini, F.; Levi, G. A Simple Apparatus for Studying the Release of Neurotransmitters from Synaptosomes. Eur. J. Pharmacol. 1974, 25, 411–414.

40. Di Prisco, S.; Merega, E.; Bonfiglio, T.; Olivero, G.; Cervetto, C.; Grilli, M.; Usai, C.; Marchi, M.; Pittaluga, A. Presynaptic, release-regulating mGlu2 -preferring and mGlu3 -preferring autoreceptors in CNS: Pharmacological profiles and functional roles in demyelinating disease. Br. J. Pharmacol. 2016, 173, 1465–1477.

41. Raiteri, L.; Raiteri, M. Synaptosomes still viable after 25 years of superfusion. Neurochem. Res. 2000, 25, 1265–1274.

42. Olivero, G.; Vergassola, M.; Cisani, F.; Usai, C.; Pittaluga, A. Immuno-Pharmacological Characterization of Presynaptic GluN3A-Containing NMDA Autoreceptors: Relevance to Anti-NMDA Receptor Autoimmune Diseases. Mol. Neurobiol. 2019, 56, 6142–6155.

43. Hou, T.J.; Wang, J.M.; Li, Y.Y.; Wang, W. Assessing the performance of the molecular mechanics/Poisson Boltzmann surface area and molecular mechanics/generalized Born surface area methods. II. The accuracy of ranking poses generated from docking. J. Comp. Chem. 2011, 32, 866–877.

44. Kollman, P.A.; Massova, I.; Reyes, C.; Kuhn, B.; Huo, S.; Chong, L.; Lee, M.; Lee, T.; Duan, Y.; Wang, W.; et al. Calculating structures and free energies of complex molecules: Combining molecular mechanics and continuum models. Acc. Chem. Res. 2000, 33, 889–897.

45. Wang, E.; Sun, H.; Wang, J.; Wang, Z.; Liu, H.; Zhang, J.Z.H.; Hou, T. End-Point Binding Free Energy Calculation with MM/PBSA and MM/GBSA: Strategies and Applications in Drug Design. Chem. Rev. 2019, 119, 9478–9508.

46. Bonfiglio, T.; Olivero, G.; Vergassola, M.; Di Cesare Mannelli, L.; Pacini, A.; Iannuzzi, F.; Summa, M.; Bertorelli, R.; Feligioni, M.; Ghelardini, C.; et al. Environmental training is beneficial to clinical symptoms and cortical presynaptic defects in mice suffering from experimental autoimmune encephalomyelitis. Neuropharmacology 2019, 145, 75–86.